Electron. Mater. Lett., Vol. 11, No. 5 (2015), pp. 862-870
DOI: 10.1007/s13391-015-5005-1

Post-Annealing Effects on the Physical and Optical Waveguiding Properties of RF Sputtered ZnO Thin Films

Faiza Meriche,[1] Tahar Touam,[2,*] Azeddine Chelouche,[3] Mohamed Dehimi,[2] Jeanne Solard,[4] Alexis Fischer,[4] Azzedine Boudrioua,[4] and Lung-Han Peng[5]

[1]Laboratoire d'Etudes des Matériaux, Université de Jijel, Jijel, 18000, Algérie
[2]Laboratoire des Semi-conducteurs, Université Badji Mokhtar-Annaba, Annaba, 23000, Algérie
[3]Laboratoire de Génie de l'Environnement, Université de Bejaia, Bejaia, 06000, Algérie
[4]Laboratoire de Physique des Lasers, Université Paris 13, Sorbonne Paris Cité, Villetaneuse, 93430, France
[5]Department of Electrical Engineering, National Taiwan University, Taipei, 106, Taiwan

(received date: 4 January 2015 / accepted date: 20 May 2015 / published date: 10 September 2015)

ZnO thin films were deposited at room temperature onto glass substrate by RF sputtering technique. Effects of the post-annealing at 300 - 500°C on the structural, morphological, optical and waveguiding properties were investigated using different characterization techniques. X-ray diffraction (XRD) analyses have shown that all thin films have a hexagonal wurtzite structure with higher *c*-axis preferred orientation (002), better crystallinity and larger crystallite size as post-annealing temperature increases. Fourier transform infrared (FTIR) spectra of annealed samples confirmed that the ZnO stretching vibration bond was found to be stable at 419 cm^{-1}. Scanning electron microscopy (SEM) and atomic force microscopy (AFM) images have revealed that film morphology and surface roughness were influenced by heat treatment temperatures. The UV-Vis-NIR spectrophotometry characterisations have indicated that all the films were highly transparent with average transmittance exceeding 81% within the visible region, and the bandgap energy of the as-deposited film was increased with increasing of the annealing temperature.The obtained results from *m*-lines spectroscopy (MLS) measurements at 632.8 nm wavelength have demonstrated that all ZnO thin film optical waveguides were single mode and the ordinary and extraordinary refractive index values of the film annealed at 500°C were very close to the corresponding ZnO single-crystal values.

Keywords: zinc oxide thin film, RF-sputtering, structure and morphology, optical waveguiding properties, photonic device applications

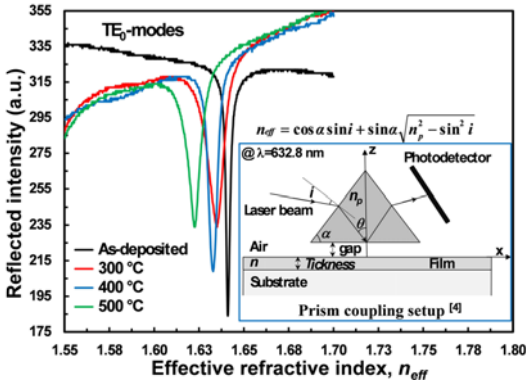

1. INTRODUCTION

Zinc oxide (ZnO) has attracted great attention during the last decades due to its many interesting characteristics including wide direct bandgap (3.37 eV at 300 K), large exciton binding energy (60 meV), material stability, high transparency in the visible wavelength, large piezoelectric constants, high refractive indices and high values of second- and third-order nonlinear optical susceptibility tensors.[1-3] With all these advantages, study of ZnO based films have been actively pursued because of their many potential applications ranging from photonic devices such as optical waveguides[4-6] to green and blue/UV light-emitting diodes,[7,8] flat panel displays,[9] solar cell windows,[10] as well as on electronic devices such as piezoelectric transducer,[8,11] surface

*Corresponding author: touamt@gmail.com

acoustic wave devices,[12,13] and transparent conducting coatings.[14]

Due to recent progress on the materials science technology, ZnO thin films can be prepared by a variety of techniques such as molecular beam epitaxy,[15] metal organic chemical vapor deposition,[16] atomic layer deposition,[17] pulsed laser deposition,[18] chemical vapor deposition[19] ultrasonic spray pyrolysis technique,[20] sol-gel process[21] and direct current and radio frequency (RF) sputtering.[22,23] Among these methods, the RF sputtering technique has attracted large attention due to its repeatability, efficiency, reliability, high deposition rates, good adhesion and high density for the deposited films. In addition, this technique produces at low substrate temperature well oriented thin films of various material compositions[24] with excellent uniformity on large area of different type of substrates.

Many works have been reported on the characterization of the structural, morphological, electrical and optical properties of sputtered ZnO thin films with various deposition parameters.[25-32] It was pointed out that the properties of ZnO thin films are influenced by the sputtering conditions such as RF power, gas pressure, growth rate, target to substrate distance, substrate temperature, substrate type, film thickness and post-deposition annealing. Furthermore, it has been shown that refractive indices of ZnO thin films deposited by RF sputtering were strongly affected by the heat treatment temperature.[5,6] Therefore, accurate determination of these optical parameters is of great importance for the design of integrated optical devices.

However, only few reports have been found regarding the use of accurate prism coupling method for the determination of optical constants of the RF-sputtered ZnO nanostructures. For example, Heideman *et al.*[5] reported the dependence of ZnO thin film optical constants, deposited on heated oxidized silicon wafer substrates at various temperatures and post-annealed in air ambient at 400°C, on the annealing time. While, Jia *et al*.[6] have estimated the refractive indices of ZnO films grown on an MgZnO buffer layer which were deposited on $LiNbO_3$ substrate and post-annealed at 400°C for 60 minutes in oxygen ambient. However, to the best of our knowledge, a systematic study, by using MLS technique,[33] of the waveguide propagating modes and the corresponding refractive indices of RF-sputtered ZnO thin films on glass substrates, as well as their dependence on the processes of post-annealing in an air atmosphere at different temperatures, has not yet been reported.

In this paper, we report the fabrication and the investigation of highly oriented single phase and transparent ZnO thin films on glass substrates by RF magnetron sputtering technique. Effects of the post-annealing treatment on the structural, morphological, optical and waveguiding properties were studied using various characterization techniques.

2. EXPERIMENTAL PROCEDURE

The ZnO thin films studied in this work were prepared at room temperature by using the RF magnetron sputtering technique. High purity ceramic targets of ZnO (99.999%) with 5.08 cm (two inches) in diameter were used for deposition on glass substrates. Prior to film deposition, the glass substrates were ultrasonically cleaned by using deionized water, ethanol and acetone for 15 min, respectively. Then, the substrates were dried in an oven at 100°C for 60 min. The sputtering chamber was initially evacuated to a base pressure of 2×10^{-6} Torr and then pure argon gas was introduced into the chamber at a flow rate of 20 sccm (standard cubic centimeters per minute). Deposition was carried out at a working pressure of 5×10^{-3} Torr after pre-sputtering for about 25 min to remove contaminants from the surface of the target. A RF power of 100 W was applied to the ZnO target while the working distance between the substrate and the target was kept at 25 cm. Under such conditions, the deposition rate of ZnO film was about of ~150 nm/hr. During the deposition, the substrate was not heated and its temperature was lower than 30°C. The as-deposited ZnO thin film was cleaved into smaller samples. These samples were annealed in an air atmosphere furnace for one hour at different temperatures ranging from 300°C to 500°C with an interval of 100°C and then cooled to room temperature before taken to the material characterization stage.

The crystalline structure of ZnO thin films, thus prepared, was characterized by using the XRD technique with a PanAlytical diffractometer. The latter was operated at 40 kV and 30 mA using Cu Kα radiation at a grazing incidence ($\omega = 0.54°$). The crystallite size of the ZnO film can be further analyzed by using the Scherrer's formula.[34] We also applied the FTIR spectroscopy to record the samples IR spectra at room temperature with a Shimadzu FTIR spectro-photometer (IRAffinity-1S). Micro-structures associated with the RF sputtered ZnO films were analyzed by the SEM technique using a Raith PIONEER System. Surface morphology of thin films in terms of root mean squared roughness (R_{rms}) was explored from the AFM images collected in a contact mode by a Nanosurf easyScan 2 operated at room temperature. The R_{rms} values used throughout this paper were calculated using the Gwyddion analysis software,[35] and are the average values based on the images collected from four different locations on the surface of each sample. The optical transmittance spectra were analyzed at room temperature by a Safas UVmc^2 UV-Visible spectrophotometer and the optical bandgap energy data was then derived from the transmission spectra. Optical waveguiding characterizations of the thin films have been carried out by MLS using a Metricon Model 2010 Prism Coupler apparatus. The film thickness of the all

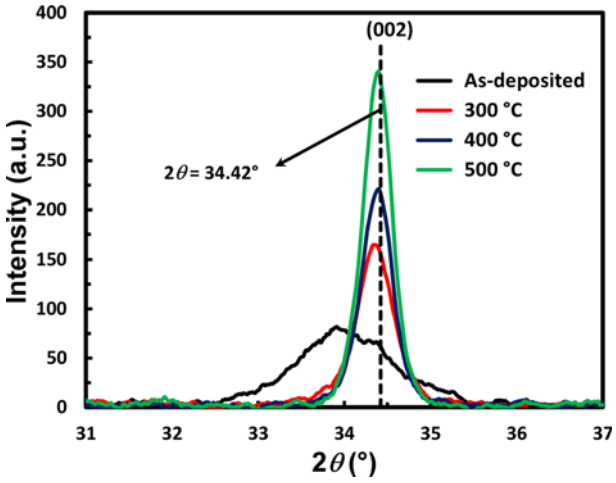

Fig. 1. XRD patterns of ZnO thin films, as-deposited and annealed for 1 h at different temperatures.

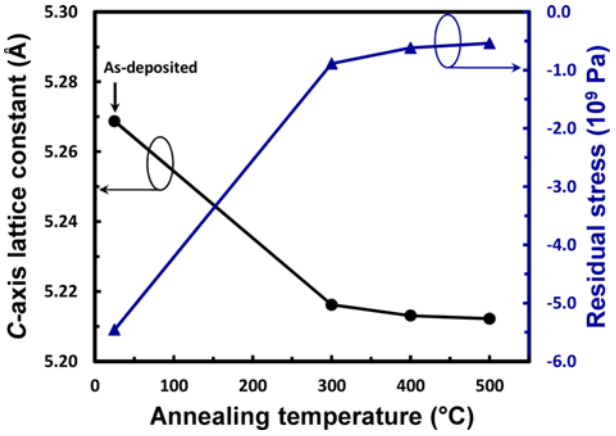

Fig. 2. C-axis lattice constant and residual stress of as-deposited and annealed ZnO thin films.

samples was measured by using a Veeco Dektak 150 Surface Profiler.

3. RESULTS AND DISCUSSION

3.1 Structural studies

The ZnO thin film structure was measured in a θ-2θ mode at a resolution of 0.017° per step size. Figure 1 displays the XRD patterns of the sputtered ZnO thin films associated with the conditions of as-deposited and annealed at different temperatures for one hour (1 h). The angular peak position of the XRD signals corresponding to bulk ZnO is indicated by a dotted line located at $2\theta = 34.42°$ according to the XRD assignment by the American Society for Testing and Materials ASTM: 36-1451. This analysis shows that all ZnO thin films are in a single phase of hexagonal wurtzite structure with a preferential growth direction along the *c*-axis which is perpendicular to the substrate surface. It is also observed that the peak XRD signal of (002) plane was shifted toward the angular value of ideal ZnO bulk peak with the increase of the annealing temperature. Our observations are in a good agreement with those reported in literature.[36] This shift indicates that the lattice constant *c* decreases with the annealing temperature, which was attributed to the residual stress effect in the sputtered ZnO thin films.[30,31] The origin of stress may be associated with the effects of sputtering atoms impacting, interstitial oxygen and/or defects in the lattice.[37]

The residual stress (σ) of the thin films can be determined from a biaxial strain model analysis.[38] Accordingly, the lattice parameters and elastic stiffness constants of the bulk ZnO are related in the following formula:

$$\sigma = -4.53 \times 10^{11} \frac{(c - c_0)}{c_0} \quad (1)$$

where $c_0 = 5.207$ Å is the unstrained lattice constant of ZnO along the *c*-axis and *c* is the lattice parameter of strained ZnO films calculated from the XRD data by means of the Bragg equation:

$$c = \frac{\lambda}{\sin\theta} \quad (2)$$

where $\lambda = 0.154056$ nm is the x-ray wavelength and θ is the Bragg angle of (002) peak.

In Figure 2, we illustrate the data of lattice constant and residual stress converted from the above analysis for the as-deposited and annealed ZnO thin films. From this figure, it was noted that with the increase of annealing temperature, the lattice parameter value was found to decrease from 5.269 to 5.212 Å and to approach to the ideal value of 5.207 Å for bulk ZnO crystal. These observations indicate that the compressive stress associated with the as-deposited ZnO film was progressively reduced with the annealing temperature up to 500°C. In particular, the as-deposited film has a stress of −5.37 GPa, while in the annealed films it gradually decreases from −0.80 GPa at 300°C to −0.45 GPa at 500°C. This suggests a thermal dynamic process by means of atomic rearrangement in the lattice structure of annealed ZnO films to release the compressive stress.[39]

To compare the micro-structure features of the ZnO thin films subject to various temperature treatment, the full-width at half-maximum (FWHM) corresponding to the XRD (002) peaks was measured and depicted in Fig. 3. A large reduction of FWHM value from 1.137° for the as-deposited film to 0.325° for the ZnO sample annealed at 500°C can be clearly discerned. This implies that the crystallinity of the ZnO films can be significantly improved by high-temperature treatment.

The average crystallite size of these *c*-axis oriented ZnO thin films can be estimated from the FWHM of (002) diffraction peak according to the well-known Scherer's formula:[34]

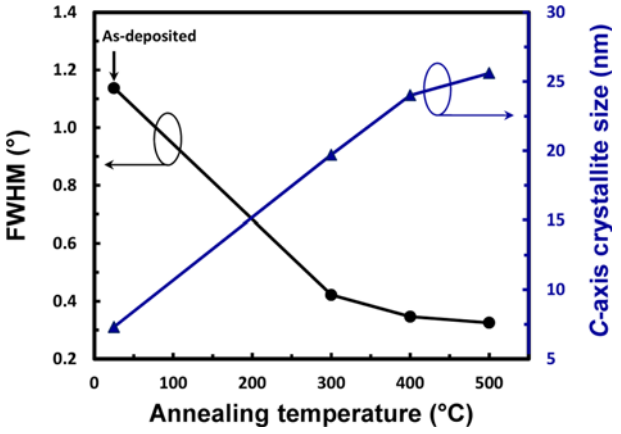

Fig. 3. FWHM and *c*-axis lattice crystallite size of as-deposited and annealed ZnO thin films.

$$D = \frac{0.89\lambda}{\beta\cos\theta} \tag{3}$$

where D is the crystallite size and β is the FWHM of the XRD signal with peak position at θ in radian.

The XRD analysis revealed that the calculated grain sizes were about 7.3, 19.7, 24.0 and 25.6 nm for the samples as-deposited and annealed at 300, 400 and 500°C, respectively. As can be seen in Fig. 3, the grain size increases with the annealing temperature, which might be due to recrystallization of the film. These observations suggest that the structural property of the thin films were improved with the increase of the annealing temperature and may be attributed to the increase of grain size and the decrease of point defects such as oxygen vacancy and zinc interstitial.

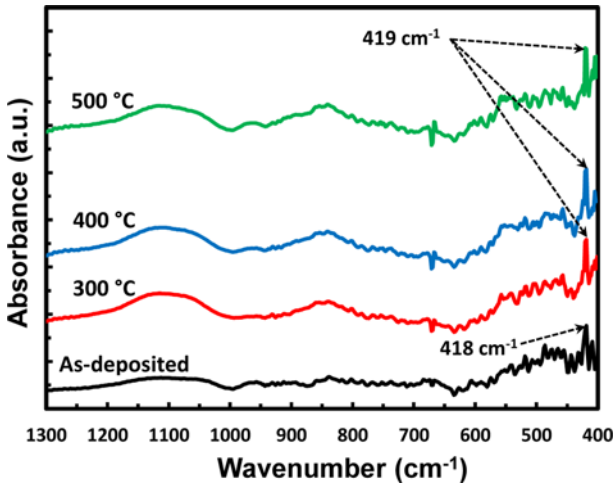

Fig. 4. Room temperature FTIR spectra of ZnO thin films, as-deposited and annealed for 1 h at different temperatures.

We further show in Fig. 4 the FTIR spectra recorded at room temperature for the ZnO thin films mentioned above. The absorbance data were taken with reference to the glass substrate used for the experiments. The as-deposited thin film exhibits an absorption peak at ~418 cm^{-1} which was assigned to the stretching vibration mode of ZnO.[40] With the increase of annealing temperature, we denote an increase of peak intensity for the aforementioned stretching vibration mode of ZnO but with energy slightly blue shifted to 419 cm^{-1}.

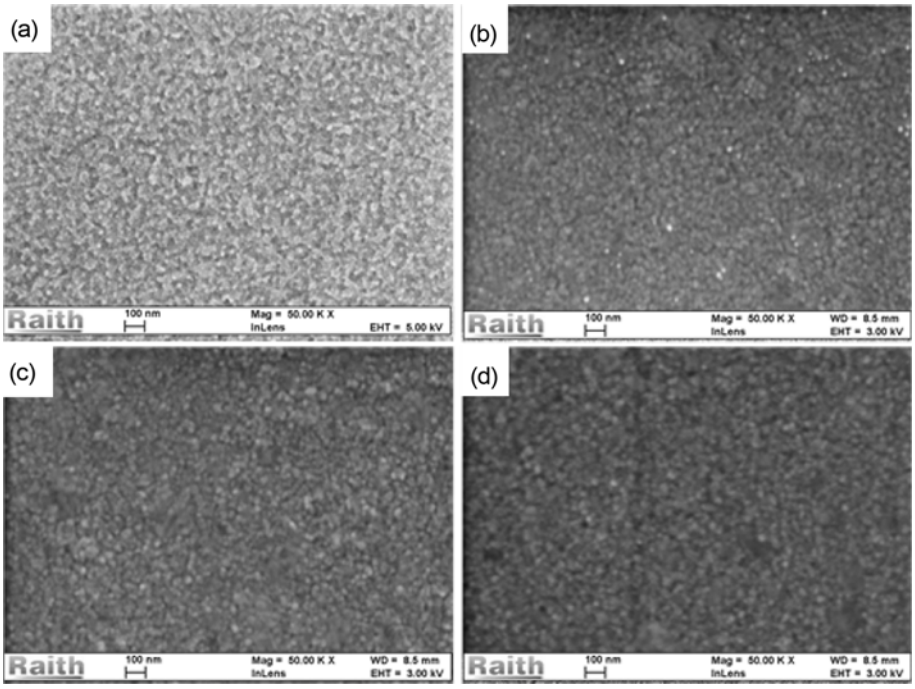

Fig. 5. SEM micrographs of ZnO thin films: (a) as-deposited, and annealed for 1 h at (b) 300°C, (c) 400°C and (d) 500°C.

As displayed in Fig. 4, the FWHM of this IR absorption band of the as-deposited thin film was found to be affected by the annealing temperature. Its width was broad (5.69 cm^{-1}) for the as-deposited films but decreases with the annealing temperature (to 0.96 cm^{-1} at 500°C), indicating the strong possession of ZnO stretching bond and the improvement in the film crystallinity.[41] The absence of any other functional peak in the spectrum confirms the good purity of the sputtered ZnO thin films. By comparing the XRD and FTIR spectra of ZnO thin films, we note that the crystallization process can be initiated at a temperature as low as 300°C, whereas it can be completed with 1 h of thermal treatment at higher annealing temperature.

3.2 Morphological analyses

The aforementioned ZnO thin films were further characterized by the SEM and AFM techniques to reveal their surface morphology and roughness. Prior to SEM imaging, all the samples were coated with a 20 - 30 nm thick conducting layer of silver to prevent the charging effect during the measurement. In Figures 5(a), (b), (c) and (d), we display the SEM micrographs (all with the same magnification) of the as-deposited samples and those of ZnO films subject to 1 h of thermal annealing at 300, 400 and 500°C, respectively. The as-deposited thin film was shown to exhibit smooth surface consisted of small spherical grain size particles. In comparison, the surface morphology of the annealed ZnO thin films was shown to be denser with the grain size enlarged with the annealing temperature. It is seen that after annealing at 500°C, the average grain size of the ZnO films is more than triple of that for the as-deposited one. This observation is in a good agreement with the estimated crystallite size values of 25.6 and 7.3 nm from XRD data analysis.

Our results are consistent with those reported in the literature.[38]

The two-dimensional (2D) and three - dimensional (3D) AFM images scanned over a surface area of 2 × 2 μm^2 for the ZnO films of as-deposited and annealed at various temperatures were further depicted in Figs. 6(a), (b), (c) and (d). The R_{rms} was calculated to be 1.14, 1.27, 1.85 and 3.22 nm for the as-deposited and the ZnO films annealed at 300, 400 and 500°C, respectively. The increase of R_{rms} with annealing temperature is mainly due to the growth of ZnO crystallite with smaller grains coalesced into larger ones. This observation was consistent with thermal analysis as revealed by the XRD characterization and SEM micrographs. Our observation also agrees with previous works[42] where it was reported that the R_{rms} value of sputtered ZnO films increased with the annealing temperature.

3.3 Optical transmittance and bandgap

The optical analyses of the ZnO thin films were explored in order to study their optical bandgap energy. Figure 7 shows the optical transmittance spectra of the as-deposited and annealed ZnO thin films measured in the 200 - 1000 nm

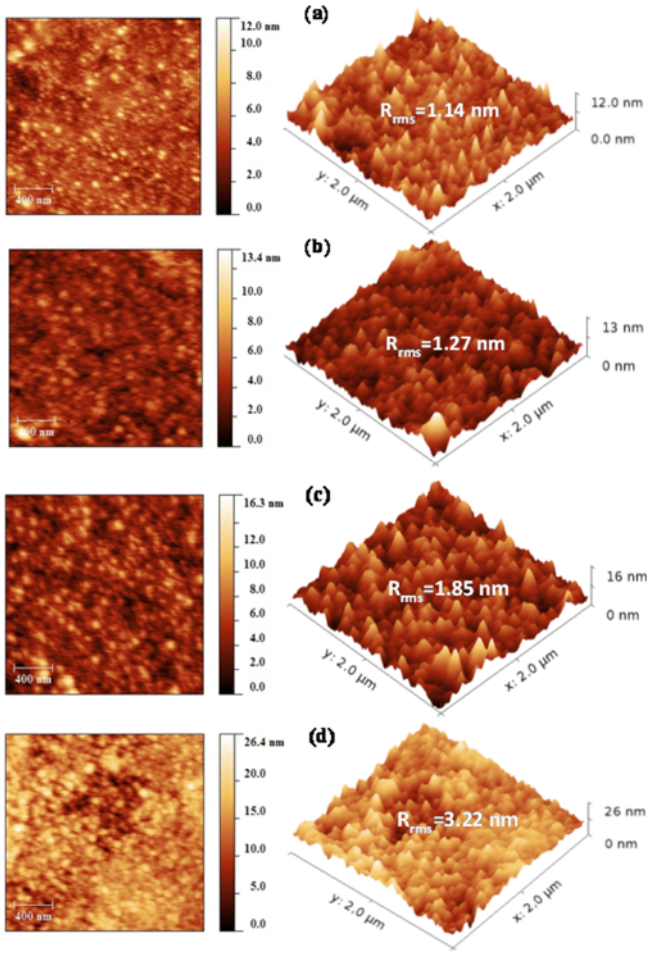

Fig. 6. 2D and 3D AFM images of ZnO films: (a) as-deposited, and annealed for 1 h at (b) 300°C, (c) 400°C and (d) 500°C.

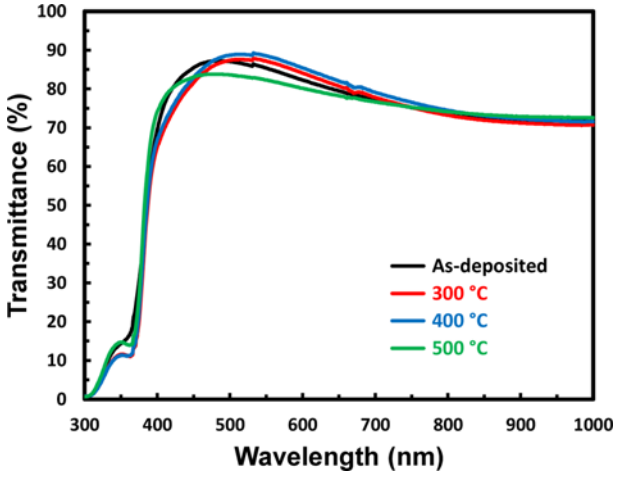

Fig. 7. Transmittance spectra of ZnO thin films, as-deposited and annealed for 1 h at different temperatures.

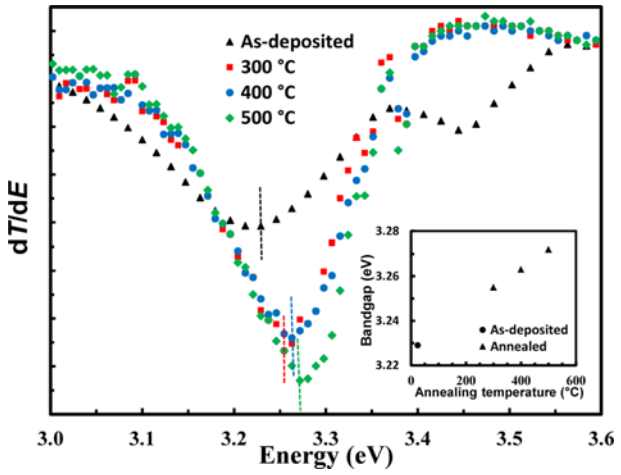

Fig. 8. Plots of the derivative of the transmittance with respect to energy of the as-deposited and annealed ZnO thin films and inset shows their corresponding bandgap values.

range. The films were highly transparent in the visible region with an average optical transmittance exceeding 81%; whereas sharp absorption edge can be found in the UV region at wavelength ranging from 370 to 405 nm. A slight fall in average transmittance was observed for the ZnO film annealed at 500°C. This may be attributed to the increase of surface roughness as revealed by AFM images.

The direct bandgap energies of all the samples were determined by using a technique based on the derivative of the transmittance (T) with respect to energy (E), dT/dE. This method has been used for analyzing the bandgap energies of semiconductors by several authors.[43,44] According to the measured transmission spectra, the dT/dE curves of ZnO thin films as-deposited and annealed at different temperature are illustrated in Fig. 8. Our analysis, depicted in insert Fig. 8, indicates that the direct optical bandgap of the as-deposited film is 3.229 eV. In comparison, the bandgap energies of the films annealed at 300, 400 and 500°C are 3.255, 3.260 and 3.272 eV, respectively. These values are very close to the ZnO bandgap value reported in the literature.[45] It can be seen that the bandgap increases with the annealing temperature. Similar trends have been also reported in the literature.[46] This shift of bandgap energy with the annealing temperature may be attributed, to the improvement in the film and the resultant reduction in the compressive stress.

3.4 Thin film waveguide characterizations

Optical properties of the ZnO films related to photonic device applications such as the waveguide propagating modes and refractive indices were further investigated by using a Metricon system (Model 2010 Prism Coupler) equipped with a He-Ne laser beam operating at a 632.8 nm wavelength. This apparatus uses the MLS technique based

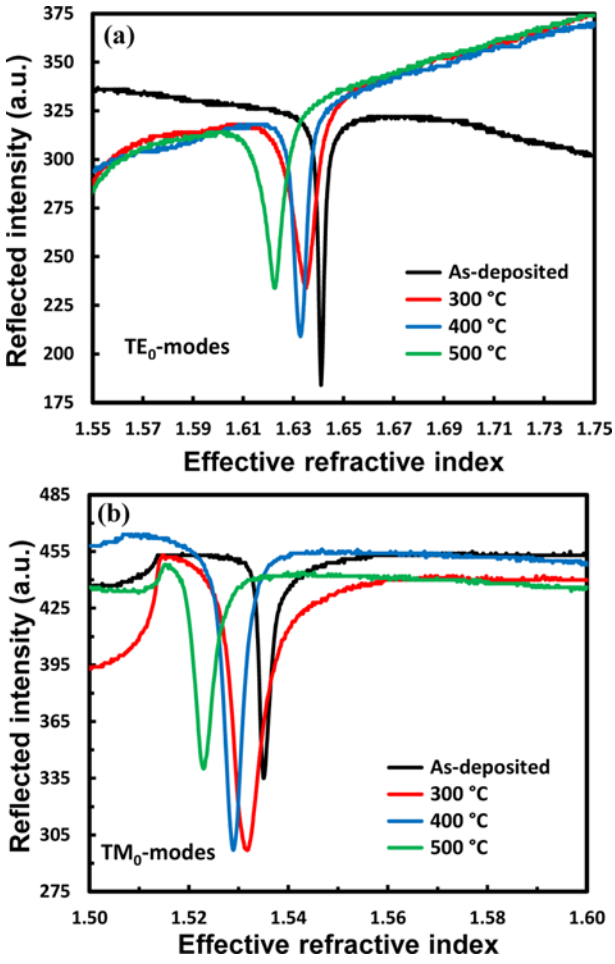

Fig. 9. Typical fundamental guided mode spectra of ZnO thin films, as-deposited and annealed for 1 h at different temperatures: (a) TE polarization and (b) TM polarization.

on the prism coupling method.[47] Procedure of applying this technique to study the aforementioned photonic properties has been described in our previous work.[33]

Figures 9(a) and (b) display the transverse electric (TE) and transverse magnetic (TM) guided mode spectra, corresponding to incident light polarization perpendicular and parallel to the c-axis respectively,[48] of the aforementioned ZnO thin films. Our results suggest that these film planar waveguides support only the fundamental TE_0- and TM_0-polarized modes. For the TE-polarization we denote that the effective mode index decreases from 1.6410 of the as-deposited ZnO thin-film planar waveguide device to 1.6225 after the device was subject to 500°C annealing. For the TM-polarization, the corresponding change in the effective mode index was from 1.5350 to 1.5230. Moreover, from the sharpness of the reflectivity dips and the FWHM of the mode spectra one can further indicate that the guided mode of the as-deposited ZnO film is better confined and would exhibit lower optical absorption losses compared to annealed

films. The latter was suggested by our previous study demonstrating that guided mode spectra with smaller FWHM have lower optical losses.[4,49] Furthermore, the annealed films are characterized with denser structure, larger grain size and rougher surface. Combination of these microstructure properties can lead to higher optical attenuation, due to the enhanced scattering losses.

The waveguide thickness of these ZnO films was measured by mechanical surface profiling and found to be about of 135.8, 132.1, 127.9 and 120.7 ± 0.2 nm for the as-deposited and annealed films at 300, 400 and 500°C, respectively. These obtained thickness values and the measured effective indices of the waveguide modes are used through the theoretical approach of MLS based on a step-index profile model for the refractive index calculations.[47] In our experiments, the ZnO film is uniaxial and characterized with ordinary (n_o) and extraordinary (n_e) refractive indices for the TE- and TM- polarization, respectively.[4,48] Data shown in Fig. 10 exhibit the correlation between the extracted values of n_o and n_e refractive indices and the film thickness as a function of the annealing temperature. The vertical error bars on the measured refractive indices displayed in Fig. 10 reveal the ±0.2 nm estimated uncertainties in the thickness of the films. As can be seen from this figure, both n_o and n_e increase with the annealing temperature while the thickness decreases. This may be explained by the fact that the packing density increases as a consequence of the further particle agglomeration during annealing treatment resulting in the enhancement of refractive indices. This is in a good agreement with previous reported results where it was found that higher annealing temperature has enhanced the formation of more closely packed crystals.[50] These observations are also consistent with the better crystallinity and the higher densification of annealed ZnO thin films revealed by XRD analysis and SEM imaging.

The birefringence (n_e-n_o) in all ZnO thin film waveguides was also calculated and was found to be about of 0.0067, 0.0112, 0.0135 and 0.0142 for as-deposited and annealed samples at 300, 400 and 500°C, respectively. These obtained values mean that the crystalline birefringence of the as-deposited film is improved after annealing treatment with the larger birefringence indicating the higher crystallinity.[6] Therefore, it can be concluded from the abovementioned results that the refractive index values of annealed ZnO thin films are found to be very close to or a slightly lower than the corresponding single-crystal values (n_o = 1.9888, n_e = 2.0050 and n_e-n_o = 0.0162).[51] For example, for the film annealed at 500°C, we have measured an ordinary refractive index of 1.9676, an extraordinary index of 1.9818 and a birefringence of 0.0142. These values are respectively 98.93%, 98.84% and 87.76% of the single-crystal values demonstrating the high optical quality of the RF-sputtered ZnO thin films.

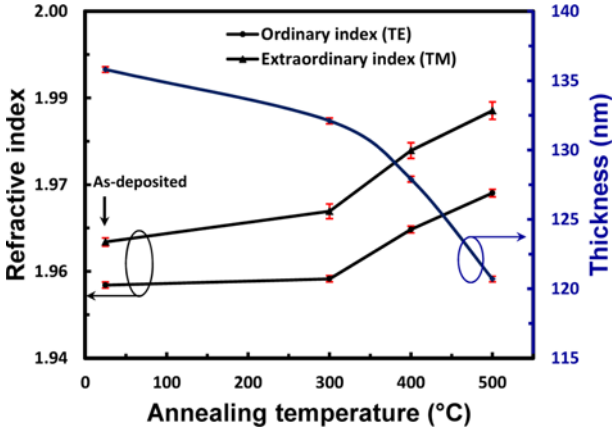

Fig. 10. Ordinary and extrordinary refractive indices and thickness of as-deposited and annealed ZnO thin films.

4. CONCLUSIONS

Highly oriented single phase and transparent ZnO thin films have been deposited on glass substrates by using RF magnetron sputtering. The effects of post-annealing treatment at 300 - 500°C on structural, morphological, optical and waveguiding properties were investigated using various characterization techniques. XRD studies have shown that the *c*-axis preferred orientation and the crystallinity of the prepared ZnO thin films were better enhanced whereas the crystallite size increases and the residual stress values significantly reduced with the increase of the annealing temperature. FTIR analysis of annealed films confirmed that the ZnO stretching vibration bond was stable at 419 cm^{-1}. SEM micrographs and AFM images have revealed that the as-deposited film was homogeneous and showed a dense structure with a very smooth surface consisting of small grain size particles, while increasing the annealing temperature leaded to a rougher films with a larger grain size. The UV-visible-NIR transmittance results showed that all the ZnO thin films were transparent with more than 81% average optical transmissions in the visible region. With an increase on the annealing temperature from 300 to 500°C, a spectral blue shift of the absorption edge from 3.255 to 3.272 eV was observed, indicating an increase in the optical bandgap energy of the as-deposited films. MLS measurements at 632.8 nm wavelength have shown that all the thin film planar waveguides were supporting only the fundamental mode for both TE- and TM- polarized light and the as-deposited film would exhibit lower propagation losses. It was found that the film thickness decreases while refractive index increases with annealing. The ordinary and extraordinary refractive indices and the birefringence values of the ZnO thin films annealed at 500°C were 98.93%, 98.84% and 87.65% of the single-crystal values indicating their high optical qualities.

ACKNOWLEDGEMENTS

The authors are grateful to Mr. L. Benidiri (University of Bejaia) for his help in the DRX characterizations and Mr. Po-Ting Lee (NTU) for preparing the ZnO films.

REFERENCES

1. V. Srikant and D. R. Clarke, *J. Appl. Phys*. **83**, 5447 (1998).
2. C. M. Frans and V. D. Pol, *Ceramic Bull.* **69**, 1959 (1990).
3. B. Kulyk, Z. Essaidi, V. Kapustianyk, B. Turko, V. Rudyk, M. Partyka, M. Addou, and B. Sahraoui, *Opt. Comm.* **281**, 6107 (2008).
4. S. Khodja, T. Touam, A. Chelouche, F. Boudjouan, D. Djouadi, Z. Hadjoub, A. Fischer, and A. Boudrioua, *Superlattices Microstruct.* **75**, 485 (2014).
5. R. G. Heideman, P. V. Lambeck, and J. G. E., *Opt. Mater.* **4**, 741 (1995).
6. C.-L. Jia, K.-M. Wang, X.-L. Wang, X.-J. Zhang, and F. Lu, *Opt. Express* **3**, 5093 (2005).
7. H. S. Kim, F. Lugo, S. J. Pearton, D. P. Norton, Y. L. Wang, and F. Ren, *Appl. Phys. Lett.* **92**, 112108 (2008).
8. H. Huang, G. Fang, X. Mo, H. Long, L. Yuan, B. Dong, X. Meng, and X. Zhao, *IEEE Electron. Dev. Lett.* **30**, 106 (2009).
9. G. M. Nam and M. S. Kwon, *J. Inf. Displ.* **9**, 8 (2008).
10. S. Major and K. L. Chopra, *Solar Ener. Mater.* **17**, 319 (1988).
11. J. Molarius, J. Kaitila, T. Pensala, and M. Ylialammi, *J. Mater. Sci.: Mater. Electr.* **14**, 431 (2003).
12. Y. Yoshio, T. Makino, Y. Katayama, and T. Hata, *Vacuum* **59**, 538 (2000).
13. W. Peng, Y. He, X. Zhao, H. Liu, X. Kang, and C. Wen, *J. Micromech. Microeng.* **23**,125008 (2013).
14. X. Yu, J. Ma, F. Ji, Y. Wang, X. Zhang, and H. Ma, *Thin Solid Films* **438**, 296 (2005).
15. D. C. Look, D. C. Reynolds, C. W. Litton, R. L. Jones, D. B. Eason, and G. Gantwell, *Appl. Phys. Lett.* **81**, 1830 (2002).
16. A. El-Yadouni, A. Boudrioua, J. C. Loulergue, V. Sallet, and R. Triboulet, *Opt. Mater.* **27**, 1391 (2005).
17. T. Tynell and M. Karppinen, *Semicond. Sci. Technol.* **29**, 043001 (2014).
18. A. A. Lotin, O. A. Novodvorsky, D. A. Zuev, O. D. Khramova, L. S. Parshina, F. V. Lebedev, J. W. Bartha, and C. Wenzel, *Opt. Mater.* **35**, 1564 (2013).
19. T. M. Barnes, J. leaf, C. Fry, and C. A. Wolden, *J. Cryst. Growth* **274**, 412 (2005).
20. Y. Bouznit, Y. Beggah, and F. Ynineb, *Appl. Surf. Sci.* **258**, 2967 (2012).
21. M. Tazerout, A. Chelouche, T. Touam, D. Djouadi, F. Boudjouan, S. Khodja, S. Ouhenia, A. Fischer, and A. Boudrioua, *Eur. Phys. J. Appl. Phys.* **67**, 10502 (2014).
22. J.-B. Lee, C.-K. Park, and J.-S. Park, *J. Korean Phys. Soc.* **50**, 1073 (2007).
23. M. A. Vasquez-A, O. Goiz, R. Baca-Arroyo, J. A. Andraca-Adame, G. Romero-Paredes, and R. Peña-Sierra, *J. Nanosci. Nanotechnol.* **12**, 234 (2012).
24. B.-Y. Oh, M.-C. Jeong, W. Lee, and J.-M. Myoung, *J. Cryst. Growth* **274**, 453 (2005).
25. V. Kapustianyk, B. Turko, A. Kostruba, Z. Sofiani, B. Derkowska, S. Dabos-Seignon, B. Barwinski, Y. Eliyashevskyi, and B. Sahraoui, *Opt. Comm.* **269**, 346 (2007).
26. Y.-J. Zhao, D.-Y. Jiang, M. Zhao, R. Deng, J.-M. Qin, S. Gao, Q.-C. Liang, and J.-X. Zhao, *Appl. Surf. Sci.* **266**, 440 (2013).
27. N. Ekem, S. Korkmaz, S. Pat, M. Z. Balbag, E. N. Cetin, and M. Ozmumcu, *Inter. J. Hydrog. Ener.* **34**, 5218 (2009).
28. E. M. Bachari, G. Baud, S. B. Amor, and M. Jacquet, *Thin Solid Films* **348**, 165 (1999).
29. Y. M. Lu, W. S. Hwang, W. Y. Liu, and J. S. Yang, *Mater. Chemis. Phys.* **72**, 269 (2001).
30. X. P. Peng, Z. G. Wang, Y. Song, T. Ji, H. Zang, Y. H. Yang, and Y. F. Jin, *Sci. China - Phys. Mech. Astron.* **50**, 281 (2007).
31. G. A. Kumar, M. V. R. Reddy, and K. N. Reddy, *Res. J. Phys. Sci.* **1**, 17 (2013).
32. J. Husna, M. M. Aliyu, M. A. Islam, P. Chelvanathan, N. R. Hamzah, M. S. Hossain, M. R. Karim, and N. Amin, *Energy Procedia* **25**, 55 (2012).
33. T. Touam, L. Znaidi, D. Vrel, O. Brinza, I. N. Kuznetsova, A. Fischer, and A. Boudrioua, *Coat.* **3**, 49 (2013).
34. J. I. Langford and A. J. C. Wilson, *J. Appl. Cryst.* **11**, 102 (1978).
35. D. Nečas and P. Klapetek, *Cent. Eur. J. Phys.* **10**, 181 (2012).
36. J.-W. Jeon, M. Kim, L.-W.Jang, J. L. Hoffman, N.-S. Kim, and I.-H. Lee, *Electron. Mater. Lett.* **8**, 27 (2012).
37. J. A. Thornton and D. W. Hoffman, *Thin Solid Films* **171**, 5 (1989).
38. M. K. Puchert, P. Y. Timbrell, and R. N. Lamb, *J. Vac. Sci. Technol. A* **14**, 2220 (1996).
39. M. Acosta, I. Riech, and E. Martín-Tovar, *Adv. Cond. Matter. Phys.* **2013**, 970976 (2013).
40. P. Bilkova, J. Zemek, B. Mitu, V. Marotta, and S. Orlando, *Appl. Surf. Sci.* **252**, 4604 (2006).
41. S.-Y. Chu, W. Water, and J.-T. Liaw, J. *Eur. Ceram. Soc.* **23**, 1593 (2003).
42. Z. B. Fang, Z. J. Yan, Y. S. Tan, X. Q. Liu, and Y. Y. Wang, *Appl. Surf. Sci.* **241**, 303 (2005).
43. C. A. Parker, J. C. Roberts, S. M. Bedair, M. J. Reed, S. X. Liu, N. A. El-Masry, and L. H. Robins, *Appl. Phys. Lett.* **75**, 2566 (1999).
44. T. Touam, M. Atoui, I. Hadjoub, A. Chelouche, B. Boudine, A. Fischer, A. Boudrioua, and A. Doghmane, *Eur. Phys. J. Appl. Phys.* **67**, 30302 (2014).
45. M.-C. Jun and J.-H. Koh, *Nanoscale Res. Lett.* **7**, 294 (2012).
46. M. F. Al-Kuhaili, I. O. Alade, and S. M. A. Durrani, *Opt. Mater. Express* **4**, 2323 (2014).

47. P. K. Tien and R. Ulrich, *J. Opt. Soc. Am.* **60**, 325 (1970).
48. C. W. Teng, J. F. Muth, Ü. Özgür, M. J. Bergmann, H. O. Everitt, A. K. Sharma, C. Jin, and J. Narayan, *Appl. Phys. Lett.* **76**, 979 (2000).
49. T. Touam, L. Znaidi, D. Vrel, I. Hadjoub, I. N. Kuznetsova, O. Brinza, A. Fischer, and A. Boudrioua, *Opt. Quant. Electron*. **46**, 23 (2014).
50. S. Yang, Y. Liu, Y. Zhang, and D. Mo, *Bull. Mater. Sci.* **33**, 209 (2010).
51. W. L. Bond, *J. Appl. Phys.* **36**, 1674 (1965).